测绘出版社 SURVEYING AND MAPPING PRESS

On-orbit Geometric Calibration of Linear Push-broom Optical Satellite Based on Sparse GCPs

Yingdong PI[1], Baorong XIE[2], Bo YANG[3,4], Yiling ZHANG[2], Xin LI[1], Mi WANG[3,4]

1. *School of Remote Sensing and Information Engineering*, *Wuhan University*, *Wuhan* 430072, *China*; 2. *Shanghai Aerospace Electronic Technology Research Institute*, *Shanghai* 201109, *China*; 3. *State Key Laboratory of Information Engineering in Surveying*, *Mapping and Remote Sensing*, *Wuhan University*, *Wuhan* 430079, *China*; 4. *Collaborative Innovation Center Of Geospatial Technology*, *Wuhan* 430079, *China*

Abstract: The paper presents a geometric calibration method based on the sparse ground control points (GCPs), aiming to the linear push-broom optical satellite. This method can achieve the optimal estimate of internal and external parameters with two overlapped image pair along the charge-coupled device (CCD), and sparse GCPs in the image region, further get rid of the dependence on the expensive calibration site data. With the calibrated parameters, the line of sight (LOS) of all CCD detectors can be recovered. This paper firstly establishes the rigorous imaging model of linear push-broom optical satellite based on its imaging mechanism. And then the calibration model is constructed by improving the internal sensor model with a viewing-angle model after an analysis on systematic errors existing in the imaging model is performed. A step-wise solution is applied aiming to the optimal estimate of external and internal parameters. At last, we conduct a set of experiments on the ZY-3 NAD camera and verify the accuracy and effectiveness of the presented method by comparison.

Key words: optical satellite; on-orbit geometric calibration; overlapped image pair; sparse GCPs; viewing-angle

Citation: Yingdong PI, Baorong XIE, Bo YANG, et al. On-orbit Geometric Calibration of Linear Push-broom Optical Satellite Based on Sparse GCPs[J]. Journal of Geodesy and Geoinformation Science, 2020, 3(1): 64-75. DOI: 10.11947/j.JGGS.2020.0107.

Revised from: Acta Geodaetica et Cartographica Sinica(Vol.48, No.2, 2019)

1 Introduction

In recent years, with the rapid development of space technology in China, the image quality of optical satellite has been improved continuously, the acquisition is more convenient, and the cost has been reduced gradually, making the optical satellitebecome an important part of high resolution earth observation system. With the improvement of spatial resolution, the clarity and resolution ability of optical satellite images are increasing, and their detailed information is more abundant. However, the imaging parameters of the satellite will change due to stress release and imaging environment changes during launch. Therefore, it is impossible to obtain accurate geometric accuracy directly using the parameters from ground laboratory calibration (for example, the geo-positioning accuracy based on laboratory calibration result is at the mile level for the ZY-3 NAD camera). Therefore, on the basis of "seeing clearly", how to achieve its "measuring accuracy" has become a key issue to give full play to the performance and application potential of high-resolution optical satellite images.

In-orbit geometric calibration is an effective means to improve the uncontrolled geometric quality of satellite images, and it is also a necessary step for geometric preprocessing of optical satellites. At present, the common geometric calibration method is to

Received date: 2018-07-12; accepted date: 2018-11-12

Foundation support: National Natural Science Foundation of China (No.41601492); SAST Foundation (No.SAST2016091); Development Program of China (No.2016YFB0501402)

First author: Yingdong PI(1992—), male, PhD, majors in aerospace photogrammetry and related application.

E-mail: piyingdong@whu.edu.cn

Corresponding author: Bo YANG

E-mail: xt000025@whu.edu.cn

use the dense ground control points (GCPs) matched from the reference data of calibration sites, and the intersection method is used to realize the high-precision calculation of the internal and external systematic error parameters. Most of the satellites in service at home and abroad were calibrated in this method. Such as SPOT-5 satellite, the CNES calibrated it in orbit using the ground calibration sites distributed around the world. After calibration, the plane positioning accuracy of single imagery reached 50 m (root mean square, RMS)[1]. For the world's first high-resolution commercial remote sensing satellite IKONOS, SpaceImaging, NASA and other organizations set up a geometric calibration group, and calibrated the geometric imaging parameters of on-board sensors satellite using Lunar lake, Railroad Valley, Dark Brooking and Denver calibration sites. Finally, the planar accuracy of about 12 m (RMS) and elevation accuracy of about 10 m (RMS) were achieved, and accuracy requirements of 1 ∶ 10 000 scale topographic mapping can be reached using a small number of GCps[2-5]. For OrbView-3 satellite, reference [6] also calibrates its panchromatic camera based on geometric calibration site, and then improves the plane positioning accuracy of a panchromatic camera to 15 m (CE90), elevation accuracy to 10 m (CE90), and compensates for the internal distortion of single image effectively[6]. In the field of on-orbit geometric calibration of optical satellites, domestic scholars have also done a lot of work. In reference [7—8], camera installation angles and viewing angle of charge-coupled device (CCD) detectors are used as the parameters to be calibrated, respectively. Using the high-precision reference data of Songshan calibration site, the on-orbit geometric calibration of the panchromatic camera of ZY-1 02C satellite is performed. The results show that the uncontrolled geometric accuracy of the image is increased from 1500 m to about 100 m after on-orbit geometric calibration[7-8]. Similarly, after the launch of ZY-3 satellite, reference [9—13] used Songshan calibration site in Henan Province to perform the geometric calibration and the accuracy verification. After calibration, the uncontrolled positioning accuracy of NAD image of ZY-3 satellite was improved to about 15 m, and it was verified that the three-line array camera of ZY-3 satellite met the design requirements of zero distortion[9-13]. Similar site-based calibration methods have been applied to many satellites at home and abroad, such as ALOS, GeoEye-1, IRS-P6, KOMPSAT-2, TH-1 and so on. Generally speaking, this method has been developed and achieved good engineering applications. However, this method has inherent shortcomings due to over-reliance on the ground calibration site. There are four main aspects: ① expensive construction and maintenance costs of calibration field increase the cost of on-orbit geometric calibration; ② with the increase of imagery width, the distribution of GCPs matched from the existing reference data can no longer cover the whole CCD, which will reduce the accuracy of on-orbit calibration undoubtedly; ③ the selection of cloud-free images in transit calibration site area is greatly affected by weather, and the long revisit period of satellite will further reduce the timeliness of on-orbit geometric calibration; ④ calibration site data are usually produced by aerial photogrammetry, so the difference between satellite images and reference data images may affect the matching accuracy, further exacerbating the geometric calibration results to a certain extent.

Aiming to the limitation of traditional methods in the absence of calibration site, this paper presents an on-orbit geometric calibration method for optical remote sensing satellites based on sparse GCPs. The relative constraints between overlapping images are introduced on the basis of the traditional calibration method. Therefore, the calibration of the camera can be achieved using the sparse GCPs and image pairs (covering the camera field of view) with an overlap of not less than 50% along the direction of CCD. In the method, the geometric relationship between overlapping images intersected by the corresponding ray can construct the geometric constraints of "detector-detector" in the camera field of view, and then realize the accurate calibration of camera without calibration site. The absolute constraints of sparse

GCPs are mainly used to calibrate external parameters, and improve the ill-condition in internal calibration caused by the lack of absolute constraints. Therefore, this method does not need to match the dense GCPs from the reference data of the calibration site. It breaks away from the dependence of traditional calibration methods on calibration site, greatly reduces the cost of on-orbit geometric calibration, and is conducive to improving the timeliness of on-orbit geometric calibration.

2 Construction of Geometric Calibration Model

2.1 Imaging model

The imaging principle of optical satellite with linear push-broom imaging is shown in Fig.1, in which $o_r-x_ry_r$, $o-xyz$ and $O-XYZ$ represent the focal plane coordinate system, camera coordinate system and J2000 coordinate system, respectively; f is focal length of the camera. The object point P is the target point taken by the detector with coordinate (x,y,z) in the camera coordinate system at a certain imaging time. At this time, the CCD arranged by the linear array obtains the gray DN value of each pixel by converting the optical signal transmitted by the central projection mode into electrical signal. While the CCD imaging, the attitude determining system ADS and the orbit measurement system (GPS system) measure the attitude of the ADS in the J2000 coordinate system and the position vector of the GPS antenna center in the WGS84 coordinate system at a certain frequency.

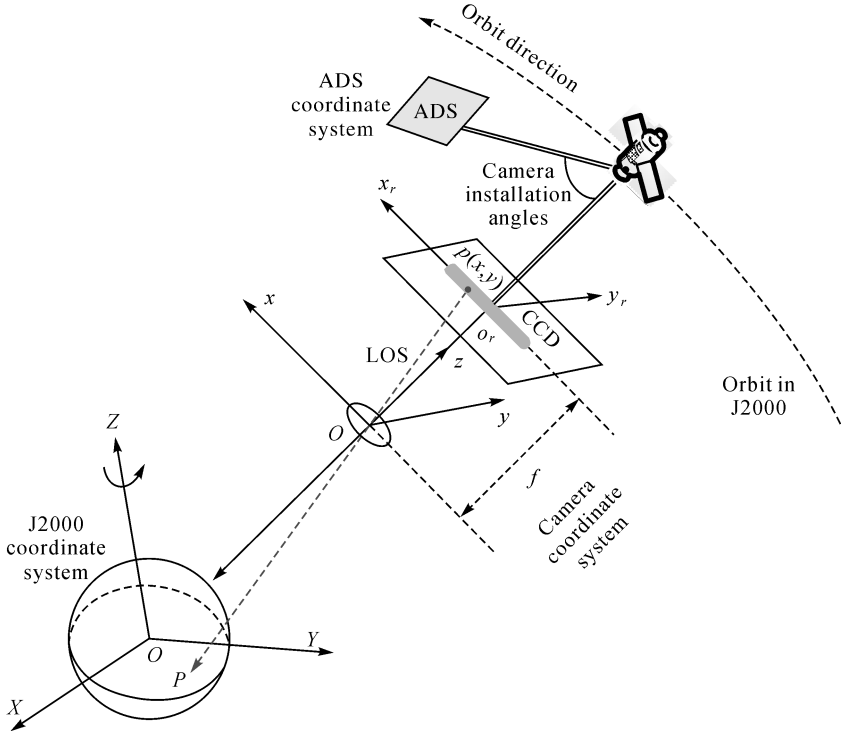

Fig.1 Imaging theory of linear push-broom optical satellite

Based on the imaging principle of linear array optical satellite, the rigorous relationship between each CCD detector and the object points taken at the imaging time can be established. The rigorous imaging model is shown in (1).

$$\begin{pmatrix} x \\ y \\ z \end{pmatrix} = \lambda R_{\text{body}}^{\text{cam}}(pitch, roll, yaw)\left(R_{\text{J2000}}^{\text{body}}(\alpha,\beta,\gamma) R_{\text{wgs}}^{\text{J2000}} \begin{bmatrix} X-X_{\text{gps}} \\ Y-Y_{\text{gps}} \\ Z-Z_{\text{gps}} \end{bmatrix}_{\text{wgs}} - \begin{bmatrix} B_X \\ B_Y \\ B_Z \end{bmatrix}_{\text{body}} \right) \tag{1}$$

In which, (x,y,z) is the coordinate of the CCD detector in camera coordinate system, (X,Y,Z) and

$(X_{\text{gps}}, Y_{\text{gps}}, Z_{\text{gps}})$ are the coordinates of ground point and the GPS antenna center in WGS84 coordinate system; $R_{\text{wgs}}^{\text{J2000}}$, $R_{\text{J2000}}^{\text{body}}$ and $R_{\text{body}}^{\text{cam}}$ are the rotation matrices from WGS84 coordinate system to J2000 coordinate system, from J2000 coordinate system to satellite body coordinate system, and from satellite body coordinate system to camera coordinate system; $(B_X, B_Y, B_Z)_{\text{body}}$ represents the coordinates of the eccentric vector from the projection center of the sensor to the phase center of the GPS antenna in the satellite body coordinate system.

2.2 Geometric calibration model

The essence of on-orbit geometric calibration is to calibrate the system error parameters that affect the accuracy of imaging model[19]. Systematic error parameters in imaging process can be divided into two categories: exterior orientation parameters (EOPs) and interior orientation parameters (IOPs). The EOPs can be generalized as the installation angle $(pitch, roll, yaw)$ between the three axes of the satellite body coordinate system and the camera coordinate system. The generalized installation matrix $R_{\text{body}}^{\text{cam}}$ based on these three angles can be used to establish the relationship between satellite and camera. The IOPs mainly include the principal point, principal distance, detector size and optical distortion parameters of the camera. Therefore, the purpose of on-orbit geometric calibration of optical satellites is to correct geometric errors in imaging models by compensating these parameters.

According to the above analysis, the parameters that need to be solved in external calibration are the three installation angles between the satellite body and the camera body, while the parameters that need to be solved in internal calibration have to be optimized to solve the problems of the rigorous camera model. The rigorous physical model is based on the imaging mechanism of optical cameras, and all kinds of parameters have clear physical significance. However, there are strong correlations between some parameters, which is particularly prominent for optical satellite cameras with narrow field of view, long focal length and linear CCD[20]. Therefore, solving these parameters directly in calibration will inevitably lead to the instability of the solution. In addition, the design technology of camera lens is complex, thus the rigorous physical model based on Brown model may have the problem of under-fitting. Therefore, this paper uses a viewing angle model as the internal calibration model, and as shown in Fig. 2, the orientation V_{image} of each CCD detector in the camera coordinate system can be precisely determined by its viewing angle (φ_x, φ_y) according to (2).

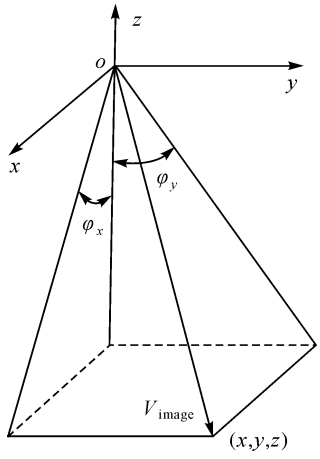

Fig.2 Viewing-angle of the CCD detector

$$\boldsymbol{V}_{\text{image}} = \left[\frac{x}{z} \quad \frac{y}{z} \quad 1\right]^{\text{T}} = \left[\tan(\varphi_x) \quad \tan(\varphi_y) \quad 1\right]^{\text{T}} \tag{2}$$

However, it is not necessary for each CCD detector to calculate its viewing angle, thus two polynomialswere be used to fit the viewing angles CCD detectors. Because of the design characteristics of optical satellites with long focal length and narrow field of view, the proportion of high-order distortion in all errors is limited. Therefore, a third-order viewing angle model is usually sufficient to accurately describe the viewing direction of each detector, as shown in (3).

$$\left.\begin{aligned}\tan(\varphi_x(s)) &= a_0 + a_1 s + a_2 s^2 + a_3 s^3 \\ \tan(\varphi_y(s)) &= b_0 + b_1 s + b_2 s^2 + b_3 s^3\end{aligned}\right\} \tag{3}$$

In which, s represents the detector number and $(a_i, b_i)(i = 0, 1, 2, 3)$ is the coefficient of the viewing angle model.

This model is the orthogonalization result of rigorous physical model, and model parameters can be

considered as a set of orthogonal bases of physical parameters. Each coefficient is equivalent to or partially equivalent to the effect of one or more physical parameters on the internal geometric distortion in a rigorous physical model. Finally, by introducing the viewing angle model into the rigorous imaging model (1), the on-orbit geometric calibration model of linear push-broom optical satellite can be constructed, as shown in (4).

$$\left.\begin{aligned} G_x &= \overline{X} - \overline{Z} \cdot \tan(\varphi_x(s)) \\ G_y &= \overline{Y} - \overline{Z} \cdot \tan(\varphi_y(s)) \end{aligned}\right\} \tag{4}$$

In which

$$\begin{bmatrix} \overline{X} \\ \overline{Y} \\ \overline{Z} \end{bmatrix} = R_{\text{body}}^{\text{cam}}(pitch, roll, yaw)\left(R_{\text{J2000}}^{\text{body}} R_{\text{wgs}}^{J2000} \begin{bmatrix} X_g - X_{\text{gps}} \\ Y_g - Y_{\text{gps}} \\ Z_g - Z_{\text{gps}} \end{bmatrix}_{\text{wgs}} - \begin{bmatrix} B_X \\ B_Y \\ B_Z \end{bmatrix}_{\text{body}}\right)$$

The unknown parameters include not only EOPs $(pitch, roll, yaw)$ and IOPs $(a_i, b_i)(i = 0, \cdots, 3)$, but also geodetic coordinates (B, L, H) of each pair of corresponding imagery points.

3 Stable Estimation of Calibration Parameters

The stepwise calculation of calibration parameters is more suitable for the proposed calibration method in this paper, and also more suitable for practical on-orbit applications. The main reasons are as follows:

The method is more suitable for separate processing because the different conditions and different models were used in the calculation of IOPs and EOPs.

For a satellite in low orbit, its parameters are stable in orbit operation. Therefore, in the life cycle of a satellite, the IOPs are usually calibrated only a few times, while the EOPs vary greatly with time. After calibration, the positioning accuracy of the image will be attenuated. It is necessary to calibrate the EOPs at a certain frequency. Therefore, the stepwise calculation of IOPs and EOPs is more suitable for practical application.

The external calibration is performed based on the sparse GCPs, and then the internal calibration is performed on the basis of the coordinate frame determined by the estimated EOPs. Internal calibration requires not only the constraints of GCPs, but also the constraints of the corresponding imagery points between images. Among them, the relative constraints of the corresponding imagery points are used to invert the high order parameters, while the absolute constraints of the GCPs are mainly used to solve the constant terms, as well as ensure the robustness solution of the internal calibration.

3.1 Estimation of EOPs based on sparse GCPs

When performing the external calibration, only the sparse GCPs of the image coverage area are needed. In this case, the initial value of the IOPs X_I^0 is taken as the true value, and the calibration model is linearized by the initial value $X_E^0 = (pitch_0, roll_0, yaw_0)$ of the EOPs. The error equation of the ith GCP can be obtained as follows:

$$V_i^E = A_i x^E - L_i^E \tag{5}$$

In which,

$$A_i = \begin{bmatrix} \dfrac{\partial G_x}{\partial pitch} & \dfrac{\partial G_x}{\partial roll} & \dfrac{\partial G_x}{\partial yaw} \\ \dfrac{\partial G_y}{\partial pitch} & \dfrac{\partial G_y}{\partial roll} & \dfrac{\partial G_y}{\partial yaw} \end{bmatrix}_i, \quad x^E = \begin{bmatrix} \Delta pitch \\ \Delta roll \\ \Delta yaw \end{bmatrix},$$

$$L_i^E = \begin{bmatrix} -G_x(X_E, X_I^0) \\ -G_y(X_E^k, X_I^0) \end{bmatrix}_{i,k},$$

x^E is the corrected value of the EOPs, L_i^E is the difference vector of the GCPs determined by the initial value X_I^0 of the IOPs and the current value X_E of EOPs.

Finally, the least squares method was used to obtain the optimal estimation of the corrected values of IOPs during the iterative estimation.

$$x^E = (M^E)^{-1} W^E \tag{6}$$

In which,

$$M^E = \sum_{i=1}^{n} A_i^T P_i^E A_i, \quad W_k^E = \sum_{i=1}^{n} A_{i,k}^T P_{i,k}^E L_{i,k}^E$$

n is the number of GCPs.

The least squares solution is an iterative process. After each iteration, the EOPs need to be updated according to the results of the solution.

When the difference between the two consecutive solutions is less than a threshold, the solution ends.

3.2 Solution of IOPs based on additional elevation constraints

Traditional methods need to match a certain number of dense GCPs uniformly distributed along the CCD to ensure the accuracy of internal calibration. Therefore, it is impossible to estimate accurately the IOPs using only the sparse GCPs. The constraints between corresponding imagery points in the overlapping images are independent of the constant terms in the IOPs, thus the solution equation is rank-deficientwhen the internal calibration is performed only using the mutual constraints of the corresponding imagery points between images. As a result, we used two kinds of constraints to solve the internal calibration. The relative constraints of corresponding imagery points were used to estimate high-order parameters, while the absolute constraints of sparse GCPs were mainly used to estimate the constant terms of IOPs, further ensuring the stability of the solution.

The internal calibration was performed on the basis of the calculated EOPs X_E in the external calibration, and then the calibration model was linearized by the initial value X_I^0 of IOPs. The error equations of GCPs were established in the same method as the external calibration. For the corresponding imagery points, the unknown parameters include not only the IOPs to be solved, but also the object coordinates of the corresponding imagery points. However, the values of the IOPs are highly correlated with the elevations corresponding to the imagery points[22-23], thus it will inevitably lead to the rank-deficient of the modified normal equation-when both of them are regarded as unknowns in the calibration solution. Aiming at this problem, additional elevation constraints were introduced to improve the condition of the solution equation. The interpolated elevation H from the reference digital elevation model (DEM) is are introduced into the model as true values to optimize the adjustment model, so as to ensure the accuracy of calibration calculation. Because the intersection condition of 50% overlapping image pairs is very weak, an opened rough grid DEM can meet the accuracy requirement of calibration, which is almost negligible compared with the high-precision reference data of calibration site.

After linearizing the model, the error equation of kth pair of corresponding imaging point can be obtained as (7):

$$V_k^I = B_k x^I + C_k t_k - L_k^I \tag{7}$$

In which,

$$B_k = \begin{bmatrix} \frac{\partial G_x^1}{\partial a_i} & \frac{\partial G_x^1}{\partial b_i} \\ \frac{\partial G_y^1}{\partial a_i} & \frac{\partial G_y^1}{\partial b_i} \\ \frac{\partial G_x^2}{\partial a_i} & \frac{\partial G_x^2}{\partial b_i} \\ \frac{\partial G_y^2}{\partial a_i} & \frac{\partial G_y^2}{\partial b_i} \end{bmatrix}_k, \quad C_k = \begin{bmatrix} \frac{\partial G_x^1}{\partial B} & \frac{\partial G_x^1}{\partial L} \\ \frac{\partial G_y^1}{\partial B} & \frac{\partial G_y^1}{\partial L} \\ \frac{\partial G_x^2}{\partial B} & \frac{\partial G_x^2}{\partial L} \\ \frac{\partial G_y^2}{\partial B} & \frac{\partial G_y^2}{\partial L} \end{bmatrix}_k,$$

$$L_k^I = \begin{bmatrix} -G_x^1(X_I, X_E) \\ -G_y^1(X_I, X_E) \\ -G_x^2(X_I, X_E) \\ -G_y^2(X_I, X_E) \end{bmatrix}_k$$

x^I is the corrections of the IOPs, t_k is the corrections of the ground plane coordinates of the corresponding imaging points. (G_x^1, G_y^1) is the calibration model for corresponding point on the left image, and (G_x^2, G_y^2) is a calibration model for corresponding point on the right image.

Finally, the error equations of GCPs and corresponding imagery points are constructed point by point by least square adjustment method, and then the modified method equation is constructed to solve the correction values of IOPs. It is the same to the solution of EOPs, and the solution of IOPs is also an iterative process. After each iteration, the IOPs need to be updated according to the results of the solution. When the difference between the two consecutive solutions is less than a threshold, the solution ends.

4 Experiments and Analysis

4.1 Introduction of experiment and data

Two sets of experiments were performed to illustrate

the effectiveness of the proposed method. The first experiment compared and analyzed the calibration results for three cases. The first case (Case1) is the proposed method of using the corresponding imagery points between overlapping images and sparse GCPs; the second case (Case2) is the calibration method using only the sparse GCPs; and the third case (Case3) is the conventional calibration site based method which uses the dense GCPs matched from the reference data of calibration sites[7-8,21]. On the basis of the calibration results, the geometric accuracy of the imaging model based on the parameters before and after calibration was verified and compared by checkpoints in the second group of experiments.

The calibration experiment was conducted on the NAD camera of ZY-3 satellite, the first civil surveying and mapping satellite in China. Two overlapping images (NAD1 and NAD2) in Nanning region of Guangxi Province were selected for calibration experiments. The additional elevation constraints were derived from the open 30 m ASTERDEM, and the overlap between imagery pairs was about 50%—60%. The traditional calibration site based method used as a scene image NAD3 covering the Songshan calibration site. The reference digital orthophoto map (DOM) and DEM are high-precision reference data covering Songshan calibration site. The resolution of DOM is 0.2 m, and the plane accuracy is better than 1 m. The resolution of DEM is 1 m, and the elevation accuracy is better than 1 m. Tab.1 lists the information of the used calibration images.

Tab.1 Information of images used for calibration

Data	Acquisition time	Area	Central longitude and latitude	Quantity of CCD probes	Resolution/m
NAD 1	2014-09-28	Nanning	108.4°E, 22.7°N	NAD:8192×3	NAD:2.1
NAD 2	2015-04-13	Nanning	108.6°E,22.7°N	FWD and BWD:	FWD and BWD:
NAD 3	2012-02-03	Songshan	113.2°E,34.4°N	4096×4	3.5

Three TDI CCDs are included in the field of view of the NAD camera of the ZY-3 satellite, but the camera adopts the optical splicing method of the semi-reflective and semi-transparent prism, and when splicing several CCD devices into a scanning line, the splicing accuracy of each CCD is better than 0.3 pixels[24]. Therefore, the multi-CCD could be directly used as a whole CCD for geometric calibration.

Four field GCPs were laid out along the line (along the track) of the image pair and measured manually on the images. In addition, the random jitter of external orientation elements would bring non-linear error to camera calibration results. In order to limit its influence and achieve the optimal fitting of geometric distortion of each CCD detector, we matched corresponding imagery points in a short area along the line (along the orbit) direction of the image pair. A high-precision matching algorithm based on SIFT operator was used to automatically match the points[25]. A total of 29830 points were obtained. Fig.3 shows the distribution of the calibrated imagery pair, the corresponding imagery points between the images and the four GCPs.

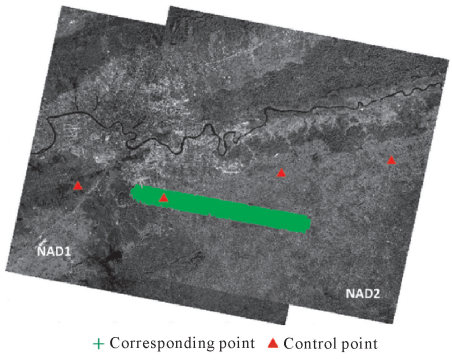

Fig.3 Distribution of ZY-3 NAD image pair and points

4.2 Calibration results

EOPs and IOPs were solved in the step-by-step method. In external calibration, only the sparse GCPswere used to estimate the EOPs, and then the sparse GCPs and the corresponding imagery points were used to calibrate the IOPs, thus the precise orientation of each CCD detector in the camera coordinate system was determined. However, due to the large number of corresponding imagery points, mis-

matching was unavoidable. Aiming to solve this problem, we eliminated gross points from the horizontal direction and the elevation direction. In the elevation direction, the points distributed in the region with too large topographic fluctuation were regarded as unreliable points. Within the four neighborhood grids of the intersection of imagery point and DSM, the point was regarded as the unreliable points to be eliminated if the difference between the maximum and minimum elevations was greater than a threshold. The threshold was set to 20 m in this paper. In the horizontal direction, the relative residuals of the corresponding imagery points in the image space were calculated, and the residuals were used as observations to detect gross errors. First, the mean and root mean square error (RMSE) of all observations were calculated, and then the corresponding imagery point whose deviation relative to the mean value is three times greater than the RMSEwas regarded as gross error and eliminated. By eliminating the errors in horizontal and elevation directions, the reliability and accuracy of the corresponding imagery points used in the calculation could be guaranteed.

Additionally, the imaging time of the two images NDA1 and NAD2 is quite different, and the EOPs change with time. In order to restrain the influence of external parameters variation on the internal calibration, we used the sparse GCPs to calibrate the two images respectively in Case 1 and Case 2, thus these two images both got a set of EOPs. In internal calibration, Case 1 used two constraints from sparse GCPs and corresponding imagery points, while Case 2 used only four sparse GCPs, but dense GCPs from calibration site was used in the internal and external calibration of Case 3. Therefore, the results obtained by Case 3 could be used as a benchmark in accuracy evaluation.

4.2.1 External calibration results

The calibrations of EOPs were performed for these three cases. Since Case 1 and Case 2 are identical in external calibration, they are not discussed separately. Finally, the results of external calibration for three cases are listed in Tab.2, in which NAD1 and NAD2 correspond to the external calibration results of Case 1 and Case 2, and NAD3 corresponds to the results of Case 3.

Tab.2 Estimated external calibration results of NAD camera

EOPs	*pitch*	*roll*	*yaw*
unit	*rad*	*rad*	*rad*
Design values	0.0	0.0	0.0
NAD1	0.001 292 035 0	−0.001 596 842 8	−0.003 240 301 1
NAD2	0.001 399 428 8	−0.001 230 866 7	−0.003 120 849 4
NAD3	0.001 339 341 8	−0.001 638 088 9	−0.003 252 521 7

4.2.2 Internal calibration results

Because the IOPs do not change significantly with time, two overlapping images with different imaging time could share a set of IOPs. On the basis of the estimated EOPs, the IOPs of the camera were calculated for the three cases respectively. The estimated IOPs are as follows:

Tab.3 Estimated internal calibration results of three cases

IOPs	Design values	Calibration results		
		Case 1	Case 2	Case 3
a_0	0.0	5.544 804E-07	9.662 450E-06	−1.110 440E-07
a_1	0.0	−2.210 579E-10	−4.622 201E-09	−5.070 804E-11
a_2	0.0	1.950 701E-14	4.960 980E-13	1.333 176E-14
a_3	0.0	−7.082 056E-19	−1.410 958E-17	−5.610 503E-19
b_0	5.050 294E-02	5.051 685E-02	5.048 926E-02	5.051 925E-02
b_1	−4.117 647E-06	−4.117 494E-06	−4.100 026E-06	−4.119 179E-06
b_2	0.0	−1.244 090E-13	−2.040 418E-12	−2.68 5835E-15
b_3	0.0	2.548 508E-18	5.575 321E-17	1.456 748E-19

4.3 Calibration accuracy evaluation and analysis

Based on the above calibration results, the accuracy of on-orbit geometric calibration was evaluated. The distortion curves of the calibrated camera and the ge-

ometric positioning accuracy are important indicators to characterize the accuracy and validity of on-orbit geometric calibration. Therefore, we verified and analyzedthe calibration method and the accuracy of the results from these two aspects. The first experiment compared and analyzed the camera internal distortionsafter calibration under three conditions. The second experiment verified the geometric positioning accuracy of images before and after calibration based on different error compensation models.

4.3.1 Contrastive analysis of camera internal distortion

Distortion curves can accurately characterize the changes of IOPs in calibration compared with their design values. Firstly, the viewing angles of each CCD detector in the camera coordinate system were calculated based on the IOPs before and after calibration. Then, the residual errors of the viewing angles of all CCD detectors in both directions (along and across the orbit) after calibration were calculated relative to the viewing angles before calibration. Finally, the distortion curves in three cases could be drawn according to the residual values, as shown in Fig.4.

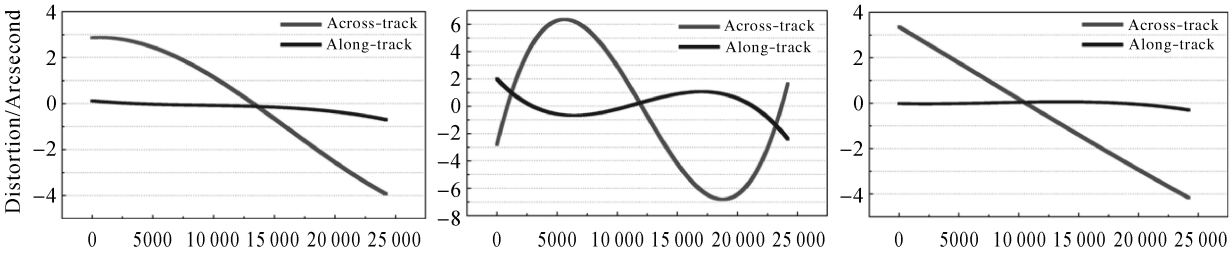

(a) Case 1 (b) Case 2 (c) Case 3

Fig.4 Internal distortion curves of NAD camera

The distortion curve obtained by the traditional method based on dense GCPs is shown in Fig.4 (c). It can be seen that the internal distortion of the NAD camera along the orbit is almost zero, while the geometric distortion of the cross the orbit is similar to a linear distortion with a fixed slope. It shows that the internal distortion of the NAD camera is mainly caused by the focal length error caused by the camera focusing after the satellite is in orbit. The conclusion confirms that the three-line array camera of ZY-3 satellite has zero distortion design. Additionally, it also shows that it is reasonable to use multi-CCD devices as a whole in this paper.

When only four sparse GCPs are used for geometric calibration, the distortion curve is shown in Figure 4 (b). Taking the distortion curve of Case 3 as the criterion, it can be found that there is still large non-linear distortion after calibration. Therefore, although the cost of acquiring a few GCPs is much lower than the cost of generating high-precision reference data of calibration site, the use of only sparse GCPs is not enough to achieve high precision results.

When the distortion curve of Case 3 is used as a criterion to evaluate the distortion curve of Case 1, it can be found that the distortion curve of Case 1 is approximately the same as that of Case 3, but there is still some non-linear distortion. The main reasonsare the elevation error introduced by internal calibration and the measurement error of the GCPs. We calculated the deviation of each CCD detector in the Case 1 relative to that of Case 3. The RMS of the deviation is 0.20 arcsec along the orbit, and 0.66 arcsec in the direction cross orbit, and the maximum deviation is less than 1.0arcsec, which generally meets the accuracy requirement better than one pixel.

4.3.2 Positioning accuracy evaluation

In order to further analyze and evaluate the effectiveness of this method in improving the geometric accuracy of NAD images, the geometric accuracy of image NAD 3 before and after calibration was compared in this experiment. Firstly, 534 uniformly dis-

tributed high-precision GCPs were matched in SIFT operator from reference data of Songshan calibration site, which were used as checkpoints to verify this accuracy. The image and the identified checkpoints are shown in Fig.5.

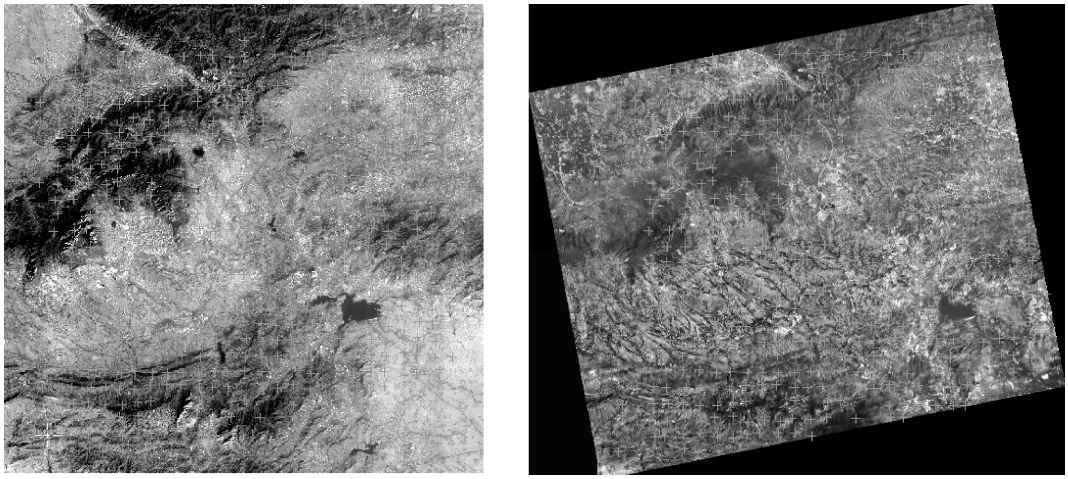

Fig.5 Validation image and check points

Then the RPC of this image was fitted based on the design values, the calibration results of Case 1 and Case 3, respectively. For Case 1, the adopted EOPs were that estimated based on NAD1 image (the imaging time of NAD1 is closer to NAD3). Finally, the imagery residuals were calculated based on the corresponding RPC under the compensation of different models. The RMS of the residuals was counted in the directions of X (cross orbit) and Y (along orbit). Then the geometric positioning accuracy of the image before and after calibration is obtained. As listed in Tab.4:

Tab.4 Geo-positioning accuracy before and after geometric calibration for NAD camera pixel

Compensation model	Before calibration		Proposed method		Calibration site method	
	X	Y	X	Y	X	Y
Without correction	399.91	324.36	14.21	10.18	0.30	0.95
Translation model	2.13	18.85	0.64	0.81	0.60	0.82
Similarity model	9.53	9.12	0.66	0.67	0.63	0.72
Affine model	0.61	0.60	0.63	0.61	0.59	0.67
Quadratic model	0.56	0.60	0.55	0.61	0.58	0.67
Cubic model	0.56	0.56	0.55	0.59	0.57	0.63

It can be seen that the positioning errors of the NAD camera in both directions are greater than 300 pixels before calibration. Even after translation transformation and similar transformation, there is still a large geo-positioning error, which indicates that there is a significant internal distortion in the image before calibration. After affine transformation correction, the positioning accuracy of the image is improved to less than one pixel. With the higher-order quadratic model and cubic model, the improvement of accuracy is not significant, which indicates that the internal distortion of NAD camera is mainly caused by the focal length error again, and the high-order optical distortion is limited.

Generally speaking, based on different error compensation models, from translationmodel to cubic model, the positioning accuracy of images before and after calibration changes from significant to stable gradually, but the two tend to stable nodes are different. For the image after calibration, the accuracy tends to be stable after using the translation model. In contrast, the image before calibration needs to be

modified by the affine model to achieve the same accuracy as the image after calibration under the translation model, and then the accuracy tends to be stable. This further shows that the image before calibration has significant distortion caused by the focal length error, and this part of the error has been significantly compensated after calibration.

After the calibration of proposed method and calibration site based method, the initial positioning error of image is significantly improved, but the positioning error of this method is still greater than 10 pixels, which is caused by the difference of imaging time between the calibration image and the validation image (the EOPs have changed). Since the adopted calibration image NAD3 in calibration site method is the same as the validation image, the initial positioning accuracy of the calibration site methodhas reached better than 1 pixel. However, this is not the point, because we are more concerned about the internal accuracy of the image. After the correction of translation model, the achieved accuracies of two methods are both better than one pixel in both directions, and they are almost the same. After the correction of higher order models, the accuracy improvement is limited for both methods, which shows that proposed method can improve the internal distortion of the image effectively, and can achieve almost the same accuracy with the calibration site method. But the lower cost and faster timeliness also show the superiority of this method over the calibration site method.

5 Conclusions

In this paper, an on-orbit geometric calibration method for optical satellites using overlapping image pairs and sparse GCPs is proposed. This method uses stepwise method to achieve high-precision solution of system error parameters, uses absolute constraints of sparse GCPs to calibrate external parameters, and ensures the robustness of internal parameters calculation. It uses relative constraints between overlapping image pairs to estimate camera high-order parameters, and finally achieves high-precision estimation of calibration parameters. The data used in this method are only two overlapping images, several uniformly distributed GCPs and open rough grid DEM, and the high-precision calibration parameters can be obtained without calibration site data. The experimental results show that this method is almost the same as the site based method in improving the geometric accuracy of satellite images, and its cost is much lower than the traditional method. In addition, the image pair required by this method does not need to consider weather factors, which greatly improves the timeliness of data acquisition compared with the calibration site image in a fixed position. However, this method still uses some GCPs, and does not achieve complete uncontrollability. Therefore, how to get rid of the control constraints completely doing internal calibration or even external calibration is our key research direction in the future.

References

[1] BOUILLON A, BERNARD M, GIGORD P, et al. SPOT5 HRS geometric performances: using block adjustment as a key issue to improve quality of DEM generation [J]. ISPRS Journal of Photogrammetry & Remote Sensing, 2006, 60: 134-146.

[2] DIAL G. Ikonos satellite mapping accuracy[C]. Ecotoxicology. 2000;371-8.

[3] GRODECKI J, LUTES J. IKONOS geometric calibrations[C]. Proc. ASPRS Annu. Conf., pp. 1-6, 2005.

[4] FRASER C S, HANLEY H B, YAMAKAWA T. High precision geopositioning from Ikonos satellite imagery. Proceedings ASPRS Annual Meeting, Washington DC, 2002.

[5] Grodecki, Jacek and Gene Dial. IKONOS geometric accuracy [C], Proceedings of Joint Workshop of ISPRS Working Groups I/2, I/5 and IV/7 on High Resolution Mapping from Space 2001, University of Hannover, Hannover, Germany, Sept19-21, 200.

[6] MULAWA D. On-orbit geometric calibration of the orb-view3 high-resolution imaging satellite[C]. ISPRS XXth Congress Proceedings. Istanbul:The International Archives of the Photogrammetry, Remote Sensing and Spatial Information Sciences,2004.

[7] YANG Bo, WANG Mi. On-orbit geometric calibration method of ZY-1 02C panchromatic camera[J]. Journal of Remote Sensing, 2013, 17(5):1175-1190.

[8] WANG M, YANG B, HU F, et al. On-orbit geometric calibration model and its applications for high-resolution optical satellite imagery [J]. Remote Sensing, 2014, 6(5):

4391-4408.

[9] LI DEREn. China's first civilian three-line-array stereo mapping satellite: ZY-3[J]. Acta Geodaetica et Cartographica Sinica, 2012, 41(3):317-322.

[10] GONG Jianya, WANG Mi, YANG Bo. High precision geometric processing theory and method of high resolution optical remote sensing satellite imagery without GCP[J]. Acta Geodaetica et Cartographica Sinica, 2017, 46(10): 1255-1261.

[11] CAO Jinshan, YUAN Xiuxiao, GONG Jianya, et al. The look-angle calibration method for on-orbit geometric calibration of ZY-3 satellite imaging sensors[J]. Acta Geodaetica et Cartographica Sinica, 2014, 43(10):1039-1045.

[12] YIFU C, XIE Z, et al. Calibration and validation of ZY-3 optical sensors. IEEE Transactions on Geoscience and Remote Sensing [J], 2015, 53(8): 4616-4626.

[13] GUO Z, YONGHUA J, et al. In-orbit geometric calibration and validation of ZY-3 linear array sensors [J]. The Photogrammetric Record, 2014, 29(145): 68-88.

[14] TAKAKU J, TADONO T. PRISM on-orbit geometric calibration and DSM performance[J]. IEEE Transactions on Geoscience & Remote Sensing, 2009, 47(12):4060-4073.

[15] MENG W, ZHU S, WEN C, et al. High accuracy on-orbit geometric calibration of linear push-broom cameras [J]. Geomatics & Information Science of Wuhan University, 2015.

[16] CRESPI M, COLOSIMO G, VENDICTIS L D, et al. GeoEye-1: analysis of radiometric and geometric capability [J]. Bose, 2010.

[17] GRUEN A, KOCAMAN S, WOLFF K. Calibration and validation of early ALOS/PRISM imagery [J]. Journal of the Japan Society of Photogrammetry & Remote Sensing, 2007, 46:24-38.

[18] RADHADEVI P V, SOLANKI S S. In-flight geometric calibration of different cameras of IRS-P6 using a physical sensor model[J]. Photogrammetric Record, 2008, 23(121):69-89.

[19] PI Y D, YANG B, WANG M, et al. On-orbit geometric calibration using a cross-image pair for the linear sensor aboard the agile optical satellite[J]. IEEE Geoscience & Remote Sensing Letters, 2017, PP(99):1-5.

[20] WANG M, CHENG Y, CHANG X, et al. On-orbit geometric calibration and geometric quality assessment for the high-resolution geostationary optical satellite GaoFen4[J]. Isprs Journal of Photogrammetry & Remote Sensing, 2017, 125:63-77.

[21] YANG B, WANG M, XU W, et al. Large-scale block adjustment without use of ground control points based on the compensation of geometric calibration for ZY-3 images[J]. Isprs Journal of Photogrammetry & Remote Sensing, 2017, 134: 1-14.

[22] YANG B, PI Y, LI X, et al. Relative geometric refinement of patch images without use of ground control points for the geostationary optical satellite GaoFen4[J]. IEEE Transactions on Geoscience & Remote Sensing, 2017, PP(99):1-11.

[23] WANG Mi, YANG Bo, JIN Shuying. A registration method based on object-space positioning consistency for satellite multi-spectral image[J].Geomatics and information science of wuhan university, 2013, 38(7):765-769.

[24] CAO Haiyi, LIU Xigang, LI Shaohui, et al.. ZY-3 satellite remote technology[J]. SPACECRAFT RECOVREY & REMOTE SENSING, 2012, 33(3):7-17.

[25] LOWE D G. Distinctive image features from scale-invariant keypoints[J]. International Journal of Computer Vision, 2004, 60(2):91-110.